

Design and fabrication of whisker hybrid ceramic membranes with narrow pore size distribution and high permeability via co-sintering process

Dong Zou ^a, Xuebin Ke ^b, Minghui Qiu ^a, Xianfu Chen ^a, Yiqun Fan ^{a*}

^a State Key Laboratory of Materials-Oriented Chemical Engineering, College of Chemical Engineering, Nanjing Tech University, Nanjing, 210009, P. R. China

^b School of Engineering and Computer Science, University of Hull, HU67RX, United Kingdom

*Corresponding author: Tel.: +86 25 83172277; Fax: +86 25 83172292.

E-mail: yiqunfan@njtech.edu.cn

Abstract

Ceramic microfiltration membranes (MF) with narrow pore size distribution and high permeability are widely used for the preparation of ceramic ultrafiltration membranes (UF) and in wastewater treatment. In this work, a whisker hybrid ceramic membrane (WHCM) consisting of a whisker layer and an alumina layer was designed to achieve high permeability and narrow pore size distribution based on the relative resistance obtained using the Hagen-Poiseuille and Darcy equations. The whisker layer was designed to prevent the penetration of alumina particles into the support and ensured a high porosity of the membrane, while the alumina layer provided a smooth surface and narrow pore size distribution. Mass transfer resistance is critical to reduce the effect of the membrane layers. It was found that the resistance of the WHCM depended largely on the alumina layer. The effect of the support and whisker layer on the resistance of the WHCM was negligible. This was consistent with theoretical calculations. The WHCM was co-sintered at 1000 °C, which resulted in a high permeability of $\sim 645 \text{ Lm}^{-1}\text{h}^{-1}\text{bar}^{-1}$ and a narrow pore size distribution of $\sim 100 \text{ nm}$. Co-sintering was carried out on a macroporous ceramic support (just needed one sintering process), which greatly reduced the preparation cost and time. The WHCM (as the sub-layer) also showed a great potential to be used for the fabrication of ceramic UF membranes with high repeatability. Hence, this study provides an efficient approach for the fabrication of advanced ceramic MF membranes on macroporous supports, allowing for rapid prototyping with scale-up capability.

Keywords: Whisker hybrid ceramic membrane; SiC whisker; Alumina particles; High permeability; Narrow pore size distribution

1 Introduction

2 Porous ceramic membranes are widely used for water purification, pollution prevention, gas separation,
3 and resource recycling [1-4]. Ceramic membranes are usually asymmetric (with “support+ intermediate
4 layer +top-layer”) [5, 6], and hence show high permeability and bending strength. The support imparts high
5 bending strengths to ceramic membranes, while the intermediate layer prevents the penetration
6 phenomenon. However, the trade-off between the permeability and filtration performance [7] of these
7 membranes limits their wide applications.

8 To alleviate the trade-off between the rejection and permeability, nanofibers/whiskers are used to
9 prevent the formation of dead-end pores in the separation layer by dividing larger voids into smaller
10 interconnected pores to improve the porosity. Generally, the porosity of nanofiber/whisker layers is more
11 than 70%, almost two times of that of traditional ceramic membranes. The network structure of the whisker
12 layer imparts high permeability and selectivity to ceramic membranes [8-11]. Wei et al.[12] used SiC
13 whiskers to decorate the surface channels of macroporous supports to prevent the penetration of top-layer
14 materials into the support. Qin et al. [13] used chitin nanowhiskers on a PVDF membrane. They found that
15 the modified membrane showed a higher pure water flux ($392 \text{ L m}^{-2} \text{ h}^{-1}$) than the undoped one (184 L m^{-2}
16 h^{-1}). Zhou et al. [14] employed attapulgite nanofibers to prepare ceramic membranes on tubular supports.
17 These nanofibers significantly improved the permeability of the resulting membranes. It was deduced that
18 the nanofibers/whiskers improved the porosity and permeability of the ceramic membranes. Furthermore,
19 the random orientation of the nanofibers reduced the number of defects and cracks generated during the
20 drying and sintering processes because of their large thermal stress resistance and high elastic modulus
21 [14].

22 Although nanofibers/whiskers improve the permeability of ceramic membranes, there are two
23 limitations in using them for the preparation of ceramic membranes. Generally, Al_2O_3 [15], ZrO_2 [16],
24 $\text{SiO}_2\text{-Al}_2\text{O}_3$ [17], and SiC [18, 19] nanofibers/whiskers are used for modifying ceramic membranes. The
25 structure of these nanofibers/whiskers is destroyed at high sintering temperatures. Furthermore, the
26 “bridging effect phenomenon” of whiskers also becomes evident. Han et al.[20] reported that at high
27 temperatures (higher than $1550 \text{ }^\circ\text{C}$), which are required for the formation of high-performance ceramics, the
28 structure of SiC whiskers is destroyed. Moreover, the porosity of the resulting ceramics decreases sharply.
29 Qiu et al.[21] investigated the effect of temperature on the structure of TiO_2 nanofibers and found that the

1 TiO₂ nanofibers could not be sintered at temperatures higher than 480 °C because of their fracture and
 2 agglomeration at high temperatures. The thermal treatment of whisker membranes is vital. The random
 3 arrangement and “bridging effect” of these whiskers make the surface of whisker membranes rough. It is
 4 difficult to fabricate separation layers for ceramic membranes with small pores (for good separation
 5 performance). Qiu et al.[21] developed nanofibers/TiO₂ sol ceramic membranes with a bi-layer structure.
 6 The sub-layer was composed of nanofibers and TiO₂ sol, while the top-layer was pure TiO₂ sol. The pure
 7 TiO₂ sol was used to modify the roughness of the sub-layer and construct the separation layer of an
 8 ultrafiltration (UF) ceramic membrane. Hence, it can be stated that the reparation process plays an
 9 important role in the fabrication of ceramic UF membranes.

10 In this study, an optimized “whisker layer + alumina layer” structure was designed on a macroporous
 11 support according to the H-P and Darcy equations to achieve WHCMs with high permeability and narrow
 12 pore size distribution, providing a comprehensive approach for the preparation of ceramic membranes on
 13 macroporous supports. The effects of the processing parameters such as the sintering temperature, SiC
 14 doping content, and reparation process on the preparation of UF membranes were studied. The schematic of
 15 the fabrication process used in this work is shown in Fig. 1. In addition, the whisker and alumina layers
 16 with the same thermodynamic properties could be co-sintered to fabricate the WHCMs, reducing the
 17 fabrication cost and time [22, 23]. The resulting WHCM was finally used as a sub-layer to fabricate
 18 ceramic UF membranes.

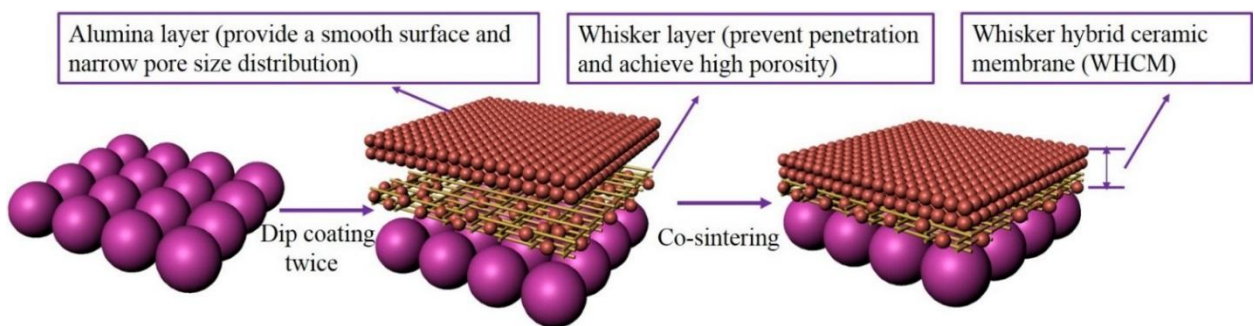


Fig. 1 Schematic of the fabrication process

2 Experimental

2.1 Materials

1 Tubular alumina support with a pore size of 1–5 μm (Length: 110 mm, External diameter: 12 mm,
 2 Thickness: 2 mm) was provided by Jiangsu Jiuwu Hi-tech Co., Ltd., and its characterization is shown in Fig.
 3 2. The average pore size was about 3 μm. Commercial SiC whiskers were used to prepare the whisker layer;

1 α -alumina particles (Sumitomo, Japan) with a mean size of 300 nm were used to prepare the alumina layer
2 to reduce the roughness of the whisker membrane.

3 **2.2 Preparation of dispersions for ceramic membrane**

4 **Dispersion A (to prepare the whisker layer):** Alumina particles (300 nm) and a nitric acid solution
5 (pH=2) were mixed thoroughly by mechanical stirring with ultrasonic treatment for 1.5 h. Desired amounts
6 of methyl cellulose (MC, Sigma), SiC whiskers, and an antifoamer were then added to the mixture under
7 stirring for another 30 min. A stable dispersion was achieved by continuing the ultrasonic treatment for
8 another 10 min for the removal of bubbles.

9 **Dispersion B (to prepare the alumina layer):** The synthesis routes of dispersions A and B were
10 similar. The only difference was that in dispersion B, SiC whiskers were not added. The solid content and
11 viscosity of dispersion B were about 25 % and 4.5 cp, respectively.

12 **Dispersion C (to prepare the UF membrane):** Boehmite sol was prepared by using a method
13 reported previously by us [24]. Al-tri-sec-butoxide (ASB, Sigma) and alcohol were first mixed, and then
14 added to hot water at 90 °C, and the resulting mixture was stirred for 60 min. A desired amount of acetic
15 acid was then added to the solution and stirring was continued for another 60 min. Finally, glycerol was
16 added to the reaction mixture, which was stirred for another 60 min. The as-prepared sol was aged for 12 h.

17 18 **2.3 Preparation of ceramic membranes**

19 **2.3.1 Preparation of WHCM**

20 First, dispersion A was coated on the surface of the ceramic support and dried for 24 h at room
21 temperature. Then, dispersion B was coated on the dispersion A coating and dried for 24 h at room
22 temperature. The WHCM was obtained after co-sintering the coatings at 1000 °C.

23 **2.3.2 Preparation of ceramic UF membrane**

24 The integrity of the WHCM was evaluated by using it (as the sub-layer) for the fabrication of UF
25 ceramic membranes. Dispersion C was coated on the WHCM. The coated WHCM was dried at room
26 temperature for 24 h and sintered at 1000 °C for 2 h. The sintering rate was 1°C/min.

27 **2.4 Characterization**

28 The X-ray diffraction patterns of the materials were obtained using an X-ray diffractometer (XRD,
29 D8-Advance, Bruker, Germany) with a scanning range of 10–80°. The surface of the membranes was
30 analyzed by using a field emission scanning electron microscope (FESEM, HitachiS-4800, Japan). The
31 roughness of the whisker layer, WHCM, and UF membrane was examined by atomic force microscopy

(AFM, 5500AFM, Agilent). The distribution of the SiC whisker and alumina particle dispersions were investigated by EDX mapping. The pore size distribution of the ceramic support was examined by mercury porosimetry. The pore size distribution of the WHCM was examined by using a self-made bubble pressure device. The permeability and rejection of the UF ceramic membrane were measured by using a self-made cross-flow filtration apparatus. The transmembrane pressure was varied from 0.1 to 0.4 MPa at 20 °C. The rejection performance of the membrane was measured using a dextran solution (6.5 g/L, molecular weight of 10000, 40000, 70000, and 500000 Da). The concentration of the feed and permeate solutions was measured by gel permeation chromatography (GPC, 1515, Waters, USA). The rejection of dextran was determined using Eq. 1

$$R_s = \frac{C_f - C_p}{C_f} \times 100\% \quad (1)$$

where C_f and C_p are the solute concentrations in the feed and permeate (g/L) solutions, respectively.

3 Results and discussion

3.1 The theoretical analysis and design process for ceramic membrane structure

In order to carry out a comprehensive research on the resistance distribution of microfiltration (MF) ceramic membranes, the effect of Φ/d_p on their resistance distribution was investigated. The calculations assumed a support with a mean pore size of 3 μm (Φ is the mean pore size of the support, and d_p is the mean particle size of the membrane material directly deposited on the support). The theoretical resistance of the membrane was calculated using the H-P (Eq. 2) [25] and Darcy (Eq. 3) [26] equations

$$J = \frac{\Delta p \cdot d_m^2 \cdot \varepsilon}{32\mu \cdot L \cdot \tau} \quad (2)$$

$$J = \frac{\Delta p}{\mu \cdot R_m} \quad (3)$$

Where Δp is the transmembrane pressure, d_m is the pore size of the membrane layer, ε is the assumed porosity of the membrane, μ is the viscosity of pure water, L is the membrane thickness, τ is the tortuosity factor, and R_m is the resistance of the membrane (m^{-1}). The following were assumed for the calculations: (1) The thickness of the penetration layer was proportional to Φ/d_p (if Φ/d_p was 10:1, the penetration layer was 10 μm); (2) The tortuosity was obtained as the reciprocal of the porosity (Eq. 4),

$$\tau = \frac{1}{\varepsilon} \quad (4)$$

1 This is consistent with the American Society for Testing and Materials testing recommendations [27] and
2 Johnston's [28] work. The value of porosity was assumed to be 0.4[29, 30]; (3) The mean pore size of the
3 membrane was calculated using its mean particle size.

$$d_p = k \cdot d_m \quad (5)$$

4 The value of k was about 3 [31, 32]. (4) The porosity of the penetration layer was a product of the porosities
5 of the support and MF membrane. Accordingly, the porosity and tortuosity of the penetration layer were
6 about 0.16 and 6.25, respectively.

7
8 **It was found that** the support and penetration layer had the lowest relative resistance when Φ/d_p was
9 2:1, indicating that coating a membrane layer with an average pore size of 500 nm on the substrate was
10 suitable (Fig. 3a). This is consistent with our previous experimental results [33]. These results provide a
11 guide to construct optimal ceramic membrane structures on macroporous supports. Fig. 3a shows that the
12 relative resistance of the penetration layer **increased with Φ/d_p** and became maximum at $\Phi/d_p = 8:1$. This
13 suggests that in order fabricate membranes with smaller pore sizes, for example 125–100 nm
14 (corresponding $\Phi/d_p = 8:1-10:1$), an extra penetration layer should be coated on the MF membrane
15 (average pore size of 500 nm) to prevent serious penetration and achieve higher permeability. Feng et al.
16 [33] first coated an alumina membrane layer (pore size of 500 nm) on a support with a mean pore size of 3
17 μm and then coated another alumina layer with a pore size of 200 nm to obtain a membrane with good
18 permeance. However, repeatable “coating-drying-sintering” processes are time consuming and costly.

19 Hence, the development of low-cost MF ceramic membranes with a small pore size (~ 100 nm) is a
20 challenge. In this study, we employed three different strategies to obtain such ceramics (Fig. 3b). The
21 resistance distribution in all the three cases was calculated using the H-P and Darcy equations. The detailed
22 parameters are listed in Table 1. It can be observed from the table that the support resistance of strategy A
23 was higher than that of strategy C owing to its smaller pore size, which can reduce the permeability of MF
24 ceramic membranes (Fig. 3c). However, strategy C exhibited an excellent resistance distribution (with
25 resistance dominated by the MF membrane) of 96.5 %. The support almost had no negative effect on the
26 permeability of the ceramic membrane (0.6 %) and the whisker layer also induced very little resistance
27 during the whole process (2.9 %), indicating that the final membrane could have a higher permeability.
28 Layers A and B showed **the** same thermodynamic properties. This is because both the layers were mainly
29 composed of alumina particles. For the fabrication of the WHCM, layers A and B **were** co-sintered to

1 reduce the sintering energy consumption. Strategy B was also not unsuitable, because the significant
2 penetration greatly increased the filtration resistance (accounted for 72.9 % of the whole process). To verify
3 the rationality of the calculations, we fabricated a WHCM experimentally with the membrane structure
4 designed using strategy C. The sintering temperature, membrane thickness, pore size distribution, and
5 permeability of the resulting membrane were investigated in detail.

6 **3.2 Effect of sintering temperature on the microstructure of the SiC whisker**

7 SiC whiskers play an important role in the fabrication of whisker membranes with better performance.
8 However, SiC whiskers easily transform to SiO₂ at higher temperatures in the presence of O₂. The sintering
9 temperature affects the morphology and structure of SiC significantly. Fig. 4 shows the morphology of the
10 SiC whiskers sintered at different temperatures. As Fig. 4 shows, at the sintering temperatures of 600, 800,
11 and 1000 °C, no significant destruction was observed in the structure of the whiskers. At 1200 °C, the SiC
12 whiskers showed serious fracture. Hence, their fabrication became difficult (Fig. 4d).

13 These phenomena can be attributed to the oxidation of the SiC whiskers, which significantly affected
14 their structure. Thermogravimetric (TG) analysis of the whiskers was carried out to analyze their oxidation
15 behavior (Fig. 5). A slight weight loss was observed in the temperature range of 500–1000 °C. However, at
16 temperatures above 1100 °C (in air) a sharp increase was observed in the weight loss. This indicates that
17 high temperatures accelerate the oxidation of SiC ($\text{SiC} + \text{O}_2 \rightarrow \text{SiO}_2 + \text{CO}_2$), which results in a serious
18 destruction of its structure. Fig. 5b shows the XRD patterns of the SiC whiskers sintered at five different
19 temperatures. No SiO₂ peak was observed within the temperature range of 600–800 °C. At the sintering
20 temperature of 1000 °C, a SiO₂ peak was observed at $2\theta = 22$ degrees, indicating that most of SiC whiskers
21 were not destroyed (a weak SiO₂ peak). The intensity of the SiO₂ peak at 22° increased gradually with an
22 increase in the temperature. Hence, SiC whiskers should be sintered in air at low temperatures (lower than
23 1000 °C) to maintain their whisker aspects.

24 **3.3 Preparation of WHCMs**

25 **3.3.1 Preparation of the whisker layer**

26 Owing to their outstanding mechanical performance, SiC whiskers [34, 35] are used to fabricate
27 whisker membranes (located in the middle of the alumina layer and substrate). These whiskers prevent the
28 penetration of alumina particles into the pores of the substrate, thus increasing the permeability of the
29 ceramic membrane. For the fabrication of the WHCMs, SiC whiskers and alumina particles were mixed to
30 prepare the whisker layer. The use of alumina particles improved the mechanical strength of the whisker
31

1 layer, as illustrated in Fig. 6. The smaller alumina particles can be formed as binders to promote the
2 sintering performance between the alumina particles and SiC whiskers, enhancing a good sintering behavior.
3 In our previous work, we also adopted alumina particles as binders (with mean particle size of 300 nm) to
4 prepare Cu-SAPO-34/monolith catalysts at low sintering temperature [36]. The SiC whiskers and alumina
5 particles can diffuse with each other at lower sintering temperature, promoting the formation of sintering
6 necks. The formation of the sintering necks can greatly improve the mechanical properties of the SiC and
7 alumina [37]. What's more, a small amount of SiO₂ (due to the slight oxidation process) occurred on the
8 surface of the SiC whiskers. The SiO₂-bonded whiskers can enhance the flexure strength [38]. Bukhari also
9 reported [39] that fabrication of SiC membrane at 1000 °C showed a satisfactory bending strength with
10 SiO₂. Under the synergy of the two mechanisms, the specimens fabricated in this work exhibit a good
11 sintering behavior and mechanical properties. The effect of the whisker content on the resulting membrane
12 was investigated. As shown in Fig. 7a, in the absence of SiC whiskers, a large number of alumina particles
13 penetrated the support because of its large pore size distribution. The thickness of the penetration layer was
14 about 10 μm, which was consistent with the hypothesis made in section 3.1. However, in the presence of
15 SiC whiskers, the membrane showed obvious structure without significant penetration (Fig. 7b).

16 The effect of the SiC whisker content on the membrane surface was investigated. The SEM images
17 (Fig. 7c) show that the membrane without whiskers (in the sub-layer) had a rough surface. This can be
18 attributed to the defects caused by the penetration of alumina particles into the substrate (in this case, the
19 sub-layer was too thin and uneven to eliminate the roughness of the substrate). On the other hand, the
20 membrane having 10 wt.% SiC whiskers showed significant whisker bridging (Fig. 7e), and no significant
21 penetration was observed on the cross-section (Fig. 7b). The SiC whiskers linked to methylcellulose
22 facilitated the formation of a giant network [29], which could block the penetration of alumina particles into
23 the substrate. At the SiC whisker content of 5 wt.%, the bridging of SiC whiskers was not significant,
24 indicating that this whisker content did not significantly contribute to the high porosity of the whisker layer
25 (Fig. 7d). However, when the whisker content was increased to 20 wt.%, dispersion A became unstable, and
26 SiC whiskers (larger than alumina particles) precipitated faster on the substrate than alumina particles,
27 resulting in the uniform distribution of SiC whiskers and alumina particles on the membrane surface (Fig.
28 7f). The optimum SiC whisker content to obtain membranes with well-dispersed SiC whiskers and high
29 porosity was found to be 10 wt.%.

30 In order to further investigate the distribution of SiC whiskers (10 wt. %) and alumina particles on the

1 membrane surface, EDX mapping was carried out (Fig. 8). It was found that Al, O, Si, and C co-existed
2 homogeneously, and Al and O were predominant. This confirmed that Al₂O₃ particles and SiC whiskers
3 were well-dispersed on the membrane surface.

4 **3.3.2 Reparation of whisker membranes by coating alumina layer**

5 The smooth surface [40] of the WHCM plays an important role in improving its anti-fouling
6 performance and in the fabrication of UF ceramic membranes (as the sub-layer). However, the whisker
7 layer had a rough surface because of the large SiC whiskers. In order to overcome this problem, an alumina
8 layer (fabricated with dispersion B) was coated on the membrane (as the intermediate layer). However, it is
9 difficult to minimize the thickness of the alumina layer during the reparation process without causing
10 defects on the membrane surface. The effect of the dipping time (60 and 90 s) of dispersion B on the
11 thickness of the alumina layer was investigated using the SEM images. Dipping for 60 s could produce an
12 alumina layer with a thickness of approximately 20 μm. On the other hand, when the dipping time was 90 s,
13 an alumina layer with a thickness of ~30 μm was obtained. The two layers (the whisker and alumina layers)
14 then were co-sintered at 1000 °C. To evaluate the integrity of the alumina layer, SEM images were used
15 (Fig. 9). The thickness (20 μm) of the alumina layer was not enough to eliminate the roughness of the
16 whisker layer. As a result, the defects in the whisker layer moved to the alumina layer, resulting in the
17 generation of macroporous defects, as shown in Fig. 9a. On the other hand, the alumina layer with a
18 thickness of about 30 μm completely eliminated the roughness of the whisker layer, resulting in the
19 formation of a homogenous top-layer without defects, as shown in Fig. 9b. The surface of the WHCM was
20 smooth with alumina particle deposits visible at high magnifications. The cross section structure of the
21 membrane was evident. The surface roughness of the whisker and alumina layers was further analyzed by
22 obtaining their AFM images (Fig. 10). From the two- and three-dimensional AFM images, **it can be clearly**
23 **observed that** the alumina layer (average roughness = 25 nm) surface was smoother than the whisker layer
24 (average roughness = 80 nm) surface (Fig. 10b). The lower surface roughness of the alumina layer made it a
25 better sub-layer for the fabrication of UF ceramic membranes.

26 On the basis of the results discussed thus far, **an optimum** WHCM was fabricated. As shown in Fig. 11,
27 the water flux of the membrane was proportional to the transmembrane pressure, and the corresponding
28 permeability of the WHCM was about 645 Lm⁻²h⁻¹bar⁻¹. The pore size distribution was narrow and the
29 mean pore size was about 100 nm. Fig. 12 compares the performance of the WHCM developed in this study
30 and those reported previously [32, 41-50]. In accordance with the H-P equation (Eq. 2), the permeability of

1 the ceramic membrane was the reciprocal of its thickness. The theoretical curve in Fig. 12 was obtained
2 when the membrane thickness was $\sim 30 \mu\text{m}$ (consistent with our final alumina layer thickness). However,
3 the previously reported values deviated from the curve. The main reason for this was that the permeability
4 of the ceramic membrane was significantly affected by the support and intermediate and top layers. The
5 resistance of support and intermediate layers accounted for above 50 % of the whole ceramic membrane,
6 and the permeability of the membrane decreased significantly. However, the permeability of the WHCM
7 was close to the curve, indicating that the WHCM showed a higher permeability with smaller pore size (100
8 nm). It is also inferred that the permeability of the WHCM is dominated by the alumina layer, having little
9 to do with the support and whisker layer. The whole process of fabricating WHCM just needed one
10 sintering process, which reduced the fabrication cost of the membrane by 20% [43].

12 3.4. Fabrication of ceramic UF membrane using WHCM as the sub-layer

13 In order to evaluate the integrity of the surface of the WHCM and widen the range of its practical
14 applications, a UF membrane was fabricated by using the WHCM. The SEM images showed that the
15 membrane surface was defect-free (Fig. 13a) and the cross-sections of the membrane were clearly
16 distinguishable and showed no penetration (Fig. 13b). The AFM images (Figs. 13c and 13d) showed that
17 the average roughness of the membrane surface was only about 3.314 nm. The rejection performance of the
18 ceramic UF membrane was measured by carrying out its dextran rejection test with a molecular weight
19 cut-off (MWCO) of 19000 Da (Fig. 13e). Based on the correlation of $r = 0.33M^{0.46}$, where r is the
20 molecular radius (nm) and M is the molar mass (kg/mol) [51], the mean pore size was calculated to be ~ 6
21 nm. The permeability of the ceramic UF membrane was about $112 \text{ Lm}^{-2}\text{h}^{-1}\text{bar}^{-1}$ (Fig. 13f).

22 Fig. 14 shows the repeatability of the fabrication of the ceramic UF membranes using the WHCM. A
23 batch of UF membranes was prepared under the optimum conditions, and 20 samples were randomly
24 selected for characterization. The MWCO was maintained within the range of 16000–21000 Da (Fig. 14a),
25 and the permeability (Fig. 14b) was maintained within the range of $110\text{--}130 \text{ Lm}^{-2}\text{h}^{-1}\text{bar}^{-1}$. It can be inferred
26 from these results that the WHCM is smooth and suitable for the fabrication of ceramic UF membranes.

28 4 Conclusion

29 In this work, the relative resistance of an MF ceramic membrane on a support with an average pore
30 size of $3 \mu\text{m}$ was analyzed using the H-P and Darcy equations. An optimum membrane structure with
31 minimum support resistance was designed. This structure was then used to fabricate the desired ceramic

1 membrane. The effect of the sintering temperature on the membrane was investigated by SEM, XRD, and
2 TG analyses. It was found that by carrying out sintering at temperatures below 1000 °C, the whisker
3 morphology of the SiC whiskers could be maintained. SiC whiskers and alumina particles were employed
4 to deposit the whisker layer on a macroporous support to prevent the penetration of alumina particles into it,
5 and thus improve the permeability of the resulting membrane. The use of alumina particles enhanced the
6 bending strength of the whisker membrane. This is because the whiskers could form sintering necks with
7 the alumina particles. The alumina layer (~30 μm) was coated on the whisker layer to eliminate its
8 roughness. The WHCM so obtained showed a high permeability of ~645 Lm⁻¹h⁻¹bar⁻¹ and a narrow pore
9 size distribution of ~100 nm, and hence was found to be suitable for the fabrication of ceramic UF
10 membranes (with high repeatability). This study provides a comprehensive approach to fabricate ceramic
11 MF membranes on macroporous supports, allowing for rapid prototyping with scale-up capability.

12

13 Acknowledgements

14 This work is financially supported by the National Natural Science Foundation of China (91534108),
15 National High Technical Research Program of China (2012AA03A606), and the Project of Priority
16 Academic Program Development of Jiangsu Higher Education Institutions (PAPD). We also appreciate Mr
17 Wei Wei for his suggestions in experimental section and Mr Guan Kecheng's meaningful discussion in this
18 work.

19

20 Reference

- 21 [1] S.K. Hubadillah, M.H.D. Othman, T. Matsuura, A.F. Ismail, M.A. Rahman, Z. Harun, J. Jaafar, M. Nomura,
22 Fabrications and applications of low cost ceramic membrane from kaolin: A comprehensive review, *Ceram. Int.*,
23 44 (2018) 4538-4560.
- 24 [2] M. Ben Ali, N. Hamdi, M.A. Rodriguez, K. Mahmoudi, E. Srasra, Preparation and characterization of new
25 ceramic membranes for ultrafiltration, *Ceram. Int.*, 44 (2018) 2328-2335.
- 26 [3] H. Verweij, *Inorganic membranes*, *Current Opinion in Chemical Engineering*, 1 (2012) 156-162.
- 27 [4] R.M. de Vos, H. Verweij, High-selectivity, high-flux silica membranes for gas separation, *Sci*, 279 (1998)
28 1710-1711.
- 29 [5] J.-W. Wang, N.-X. Li, Z.-R. Li, J.-R. Wang, X. Xu, C.-S. Chen, Preparation and gas separation properties of

- 1 Zeolitic imidazolate frameworks-8 (ZIF-8) membranes supported on silicon nitride ceramic hollow fibers, *Ceram.*
2 *Int.*, 42 (2016) 8949-8954.
- 3 [6] B. Das, B. Chakrabarty, P. Barkakati, Preparation and characterization of novel ceramic membranes for
4 micro-filtration applications, *Ceram. Int.*, 42 (2016) 14326-14333.
- 5 [7] H.B. Park, J. Kamcev, L.M. Robeson, M. Elimelech, B.D. Freeman, Maximizing the right stuff: The trade-off
6 between membrane permeability and selectivity, *Sci*, 356 (2017).
- 7 [8] X.B. Ke, H.Y. Zhu, X.P. Gao, J.W. Liu, Z.F. Zheng, High-performance ceramic membranes with a separation
8 layer of metal oxide nanofibers, *Adv. Mater.*, 19 (2007) 4325-4325.
- 9 [9] X. Ke, Z.F. Zheng, H.W. Liu, H.Y. Zhu, X.P. Gao, L.X. Zhang, N.P. Xu, H. Wang, H.J. Zhao, J. Shi, K.R.
10 Ratinac, High-flux ceramic membranes with a nanomesh of metal oxide nanofibers, *J. Phys. Chem. B*, 112 (2008)
11 5000-5006.
- 12 [10] X. Peng, J. Jin, E.M. Ericsson, I. Ichinose, General method for ultrathin free-standing films of nanofibrous
13 composite materials, *J. Am. Chem. Soc.*, 129 (2007) 8625-8633.
- 14 [11] X.B. Ke, R.F. Shao, H.Y. Zhu, Y. Yuan, D.J. Yang, K.R. Ratinac, X.P. Gao, Ceramic membranes for
15 separation of proteins and DNA through in situ growth of alumina nanofibres inside porous substrates, *Chem.*
16 *Commun.*, (2009) 1264-1266.
- 17 [12] W. Wei, W. Zhang, Q. Jiang, P. Xu, Z. Zhong, F. Zhang, W. Xing, Preparation of non-oxide SiC membrane
18 for gas purification by spray coating, *J. Membr. Sci.*, (2017).
- 19 [13] A. Qin, X. Li, X. Zhao, D. Liu, C. He, Preparation and characterization of nano-chitin whisker reinforced
20 PVDF membrane with excellent antifouling property, *J. Membr. Sci.*, 480 (2015) 1-10.
- 21 [14] S. Zhou, A. Xue, Y. Zhang, X. Huang, M. Li, Y. Zhao, Y. Fan, W. Xing, Preparation of a new ceramic
22 microfiltration membrane with a separation layer of attapulgite nanofibers, *Mater. Lett.*, 143 (2015) 27-30.
- 23 [15] Y. Tamura, B. Malmal Moshtaghioun, D. Gomez-Garcia, A. Dominguez Rodriguez, Spark plasma sintering
24 of fine-grained alumina ceramics reinforced with alumina whiskers, *Ceram. Int.*, 43 (2017) 658-663.
- 25 [16] Y.-h. Fang, X.-r. Zhao, M.-x. Zhang, P. Zhang, L. Zhang, H. Cheng, J.-b. Wu, S.-s. Feng, Preparation and
26 characterization of monoclinic rod-shaped ZrO₂ whiskers via sulfate flux, *Ceram. Int.*, 44 (2018) 10094-10098.
- 27 [17] M. Chen, L. Zhu, Y. Dong, L. Li, J. Liu, Waste-to-Resource Strategy To Fabricate Highly Porous
28 Whisker-Structured Mullite Ceramic Membrane for Simulated Oil-in-Water Emulsion Wastewater Treatment,
29 *Acs Sustainable Chemistry & Engineering*, 4 (2016).
- 30 [18] Y. Luo, S. Zheng, S. Ma, C. Liu, J. Ding, X. Wang, Novel two-step process for synthesising beta-SiC

- 1 whiskers from coal fly ash and water glass, *Ceram. Int.*, 44 (2018) 10585-10595.
- 2 [19] L. Cao, J. Liu, J. Huang, L. Zhou, X. Yong, X. Shen, L. Kong, C. Yao, Mullite whisker toughened mullite
3 coating to enhance the thermal shock resistance of SiC pre-coated carbon/carbon composites, *Ceram. Int.*, 43
4 (2017) 16512-16517.
- 5 [20] F. Han, Z. Zhong, Y. Yang, W. Wei, F. Zhang, W. Xing, Y. Fan, High gas permeability of SiC porous
6 ceramics reinforced by mullite fibers, *J. Eur. Ceram. Soc.*, 36 (2016) 3909-3917.
- 7 [21] M. Qiu, S. Fan, Y. Cai, Y. Fan, N. Xu, Co-sintering synthesis of bi-layer titania ultrafiltration membranes
8 with intermediate layer of sol-coated nanofibers, *J. Membr. Sci.*, 365 (2010) 225-231.
- 9 [22] J. Zhu, G. Zhang, G. Liu, Z. Liu, W. Jin, N. Xu, Perovskite Hollow Fibers with Precisely Controlled Cation
10 Stoichiometry via One-Step Thermal Processing, *Adv. Mater.*, 29 (2017).
- 11 [23] D. Zou, M.H. Qiu, X.F. Chen, Y.Q. Fan, One-step preparation of high-performance bilayer alpha-alumina
12 ultrafiltration membranes via co-sintering process, *J. Membr. Sci.*, 524 (2017) 141-150.
- 13 [24] X. Chen, W. Zhang, Y. Lin, Y. Cai, M. Qiu, Y. Fan, Preparation of high-flux gamma-alumina nanofiltration
14 membranes by using a modified sol-gel method, *Microporous Mesoporous Mater.*, 214 (2015) 195-203.
- 15 [25] X.B. Ding, Y.Q. Fan, N.P. Xu, A new route for the fabrication of TiO₂ ultrafiltration membranes with
16 suspension derived from a wet chemical synthesis, *J. Membr. Sci.*, 270 (2006) 179-186.
- 17 [26] W. Li, W. Xing, N. Xu, Modeling of relationship between water permeability and microstructure parameters
18 of ceramic membranes, *Desalination*, 192 (2006) 340-345.
- 19 [27] A. F902, Average circular-capillary equivalent pore diameter in filter media, (1990).
- 20 [28] P.R. Johnston, Fluid sterilization by filtration buffalo grove, III, Interpharm Press, IL, USA, (1992).
- 21 [29] W. Qin, K. Guan, B. Lei, Y. Liu, C. Peng, J. Wu, One-step coating and characterization of alpha-Al₂O₃
22 microfiltration membrane, *J. Membr. Sci.*, 490 (2015) 160-168.
- 23 [30] H. Qi, Y. Fan, W. Xing, L. Winnubst, Effect of TiO₂ doping on the characteristics of macroporous Al₂O₃
24 /TiO₂ membrane supports, *J. Eur. Ceram. Soc.*, 30 (2010) 1317-1325.
- 25 [31] S.H. Lee, K.C. Chung, M.C. Shin, J.I. Dong, H.S. Lee, K.H. Auh, Preparation of ceramic membrane and
26 application to the crossflow microfiltration of soluble waste oil, *Mater. Lett.*, 52 (2002) 266-271.
- 27 [32] C. Yang, G.S. Zhang, N.P. Xu, J. Shi, Preparation and application in oil-water separation of
28 ZrO₂/alpha-Al₂O₃ MF membrane, *J. Membr. Sci.*, 142 (1998) 235-243.
- 29 [33] J. Feng, Y. Fan, H. Qi, N. Xu, Co-sintering synthesis of tubular bilayer α -alumina membrane, *J. Membr. Sci.*,
30 288 (2007) 20-27.

1
2
3
4
5
6
7
8
9
10
11
12
13
14
15
16
17
18
19
20
21
22
23
24
25
26
27
28
29
30
31
32
33
34
35
36
37
38
39
40
41
42
43
44
45
46
47
48
49
50
51
52
53
54
55
56
57
58
59
60
61
62
63
64
65

[34] J. Zheng, M.J. Kramer, M. Akinc, In situ Growth of SiC Whisker in Pyrolyzed Monolithic Mixture of AHPCS and SiC, *J. Am. Ceram. Soc.*, 83 (2010) 2961-2966.

[35] H. Feng, Z. Zhong, Z. Feng, W. Xing, Y. Fan, Preparation and Characterization of SiC Whisker-Reinforced SiC Porous Ceramics for Hot Gas Filtration, *Ind. Eng. Chem. Res.*, 54 (2015) 226-232.

[36] X. Kong, M. Qiu, A. Wang, L. Yang, R. Zhou, Y. Fan, D. Kong, C. Gu, Influence of alumina binders on adhesion and cohesion during preparation of Cu-SAPO-34/monolith catalysts, *International Journal of Applied Ceramic Technology*, (2018).

[37] Y. Yang, F. Han, W. Xu, Y. Wang, Z. Zhong, W. Xing, Low-temperature sintering of porous silicon carbide ceramic support with SDBS as sintering aid, *Ceram. Int.*, 43 (2017) 3377-3383.

[38] J.H. She, J.F. Yang, N. Kondo, T. Ohji, S. Kanzaki, Z.Y. Deng, High-strength porous silicon carbide ceramics by an oxidation-bonding technique, *J. Am. Ceram. Soc.*, 85 (2002) 2852-2854.

[39] S.Z.A. Bukhari, J.-H. Ha, J. Lee, I.-H. Song, Effect of different heat treatments on oxidation-bonded SiC membrane for water filtration, *Ceram. Int.*, 44 (2018) 14251-14257.

[40] R. Bi, Q. Zhang, R. Zhang, Y. Su, Z. Jiang, Thin film nanocomposite membranes incorporated with graphene quantum dots for high flux and antifouling property, *J. Membr. Sci.*, 553 (2018) 17-24.

[41] P. Wang, P. Huang, N. Xu, J. Shi, Y.S. Lin, Effects of sintering on properties of alumina microfiltration membranes, *J. Membr. Sci.*, 155 (1999) 309-314.

[42] Y. Yu, W. Hou, X. Hu, Y. Yu, L. Mi, L. Song, Superhydrophobic modification of an Al₂O₃ microfiltration membrane with TiO₂ coating and PFDS grafting, *Rsc Advances*, 4 (2014) 48317-48321.

[43] Y. Lin, D. Zou, X. Chen, M. Qiu, H. Kameyama, Y. Fan, Low temperature sintering preparation of high-permeability TiO₂/Ti composite membrane via facile coating method, *Appl. Surf. Sci.*, 349 (2015) 8-16.

[44] Q. Chang, J.-e. Zhou, Y. Wang, J. Wang, G. Meng, Hydrophilic modification of Al₂O₃ microfiltration membrane with nano-sized gamma-Al₂O₃ coating, *Desalination*, 262 (2010) 110-114.

[45] C. Song, T. Wang, Y. Pan, J. Qiu, Preparation of coal-based microfiltration carbon membrane and application in oily wastewater treatment, *Sep. Purif. Technol.*, 51 (2006) 80-84.

[46] I. Jedidi, S. Saidi, S. Khemakhem, A. Larbot, N. Elloumi-Ammar, A. Fourati, A. Charfi, A.B. Salah, R.B. Amar, Elaboration of new ceramic microfiltration membranes from mineral coal fly ash applied to waste water treatment, *J. Hazard. Mater.*, 172 (2009) 152-158.

[47] Y. Dong, S. Chen, X. Zhang, J. Yang, X. Liu, G. Meng, Fabrication and characterization of low cost tubular mineral-based ceramic membranes for micro-filtration from natural zeolite, *J. Membr. Sci.*, 281 (2006) 592-599.

1
2
3
4
5
6
7
8
9
10
11
12
13
14
15
16
17
18
19
20
21
22
23
24
25
26
27
28
29
30
31
32
33
34
35
36
37
38
39
40
41
42
43
44
45
46
47
48
49
50
51
52
53
54
55
56
57
58
59
60
61
62
63
64
65

[48] R.V. Kumar, A.K. Ghoshal, G. Pugazhenthii, Elaboration of novel tubular ceramic membrane from inexpensive raw materials by extrusion method and its performance in microfiltration of synthetic oily wastewater treatment, *J. Membr. Sci.*, 490 (2015) 92-102.

[49] A. Bouazizi, M. Breida, A. Karim, B. Achiou, M. Ouammou, J.I. Calvo, A. Aaddane, K. Khiat, S. Alami Younssi, Development of a new TiO₂ ultrafiltration membrane on flat ceramic support made from natural bentonite and micronized phosphate and applied for dye removal, *Ceram. Int.*, 43 (2017) 1479-1487.

[50] H.J. Yeom, C.K. Su, Y.W. Kim, I.H. Song, Processing of alumina-coated clay–diatomite composite membranes for oily wastewater treatment, *Ceram. Int.*, 42 (2016) 5024-5035.

[51] P. Puhlfurss, A. Voigt, R. Weber, M. Morbe, Microporous TiO₂ membranes with a cut off < 500 Da, *J. Membr. Sci.*, 174 (2000) 123-133.

1 List of Tables

2 **Table 1** The parameters in the theoretical calculations process

	d_m (nm)	ε	μ (Pa.s)	τ	L (μm)	Resistance (m^{-1})
Strategy A						
Support (1 μm)						0.67
Layer A	100	0.4	0.001	2.5	30	1.67
Strategy B						
Support (3 μm)						0.05
Layer A	100	0.16	0.01	6.25	10	3.47
Layer B	100	0.4	0.001	2.5	30	1.67
Strategy C						
Support (3 μm)						0.05
Layer A	1000	0.6	0.001	1.7	30	0.01
Layer B	100	0.4	0.001	2.5	30	1.67

3

4

List of Figures

Fig.1 Schematic of the fabrication process

Fig.2 The pore size distribution of the support

Fig.3 (a) the relative resistance Vs the Φ/d_p (b) three strategies for the sub-layer (strategy A, strategy B and strategy C) (c) the relative resistance of ceramic membrane from three different strategies

Fig.4 The morphology of SiC whiskers sintered at different temperatures (a) 600 °C (b) 800 °C (c) 1000 °C (d) 1200°C

Fig.5 (a) TG of the SiC whisker (b) XRD patterns of the SiC whiskers at different sintering temperatures

Fig.6 Schematic illustration of the whiskers sintered with the aid of alumina powders with average particle size of 300 nm

Fig.7 The effect of SiC whisker doping content on the ceramic membrane (a) Cross section of doping 0 wt.% SiC whisker (b) Cross section of doping 10 wt.% SiC whiskers (c) 0 wt.% (d) 5 wt.% (e) 10 wt.% (f) 20 wt.%

Fig.8 The elements distribution on whisker membrane surface (Al, O, C and Si)

Fig.9 The effect of the dipping time on structure of membrane surface and cross section (a) 60 s (b) 90 s

Fig.10 The roughness membrane surface (a) Whisker layer (b) Alumina layer

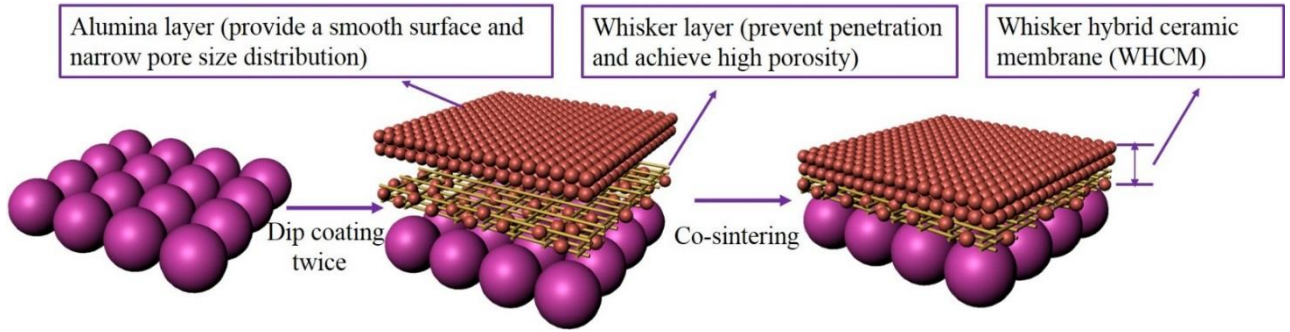
Fig.11 The performance of the WHCM (a) Permeability (b) Pore size distribution

Fig.12 The performance of the WHCM compared with the literatures

Fig.13 The SEM images of the UF membranes (a) The surface images (b) The cross section (c) 2D-AFM image (d) 3D-AFM image of membrane surface (e) Rejection performance (f) Permeability

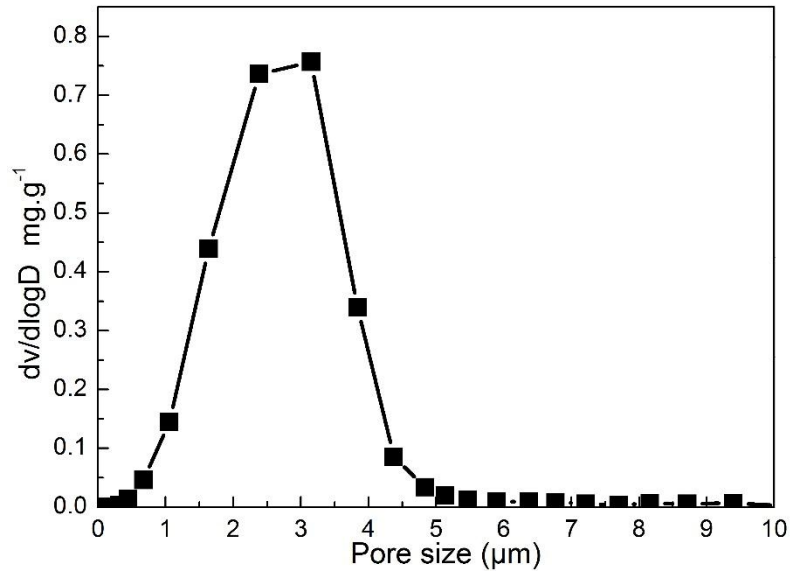
Fig.14 The repeatability of the UF membranes (a) MWCO (b) Permeability

1 **Fig.1**



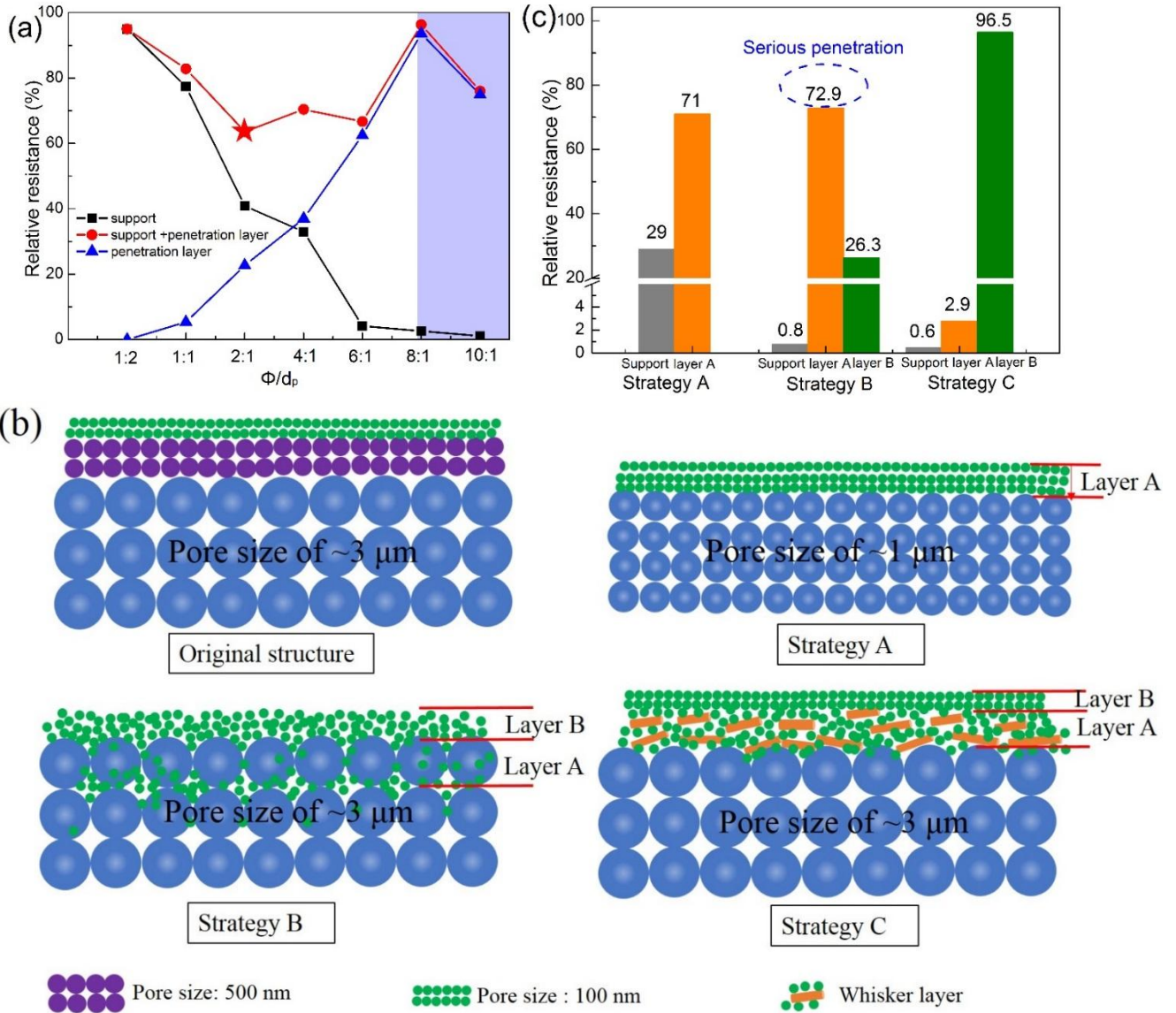
2
3
4
5
6
Fig. 1 Schematic of the fabrication process

1 **Fig.2**



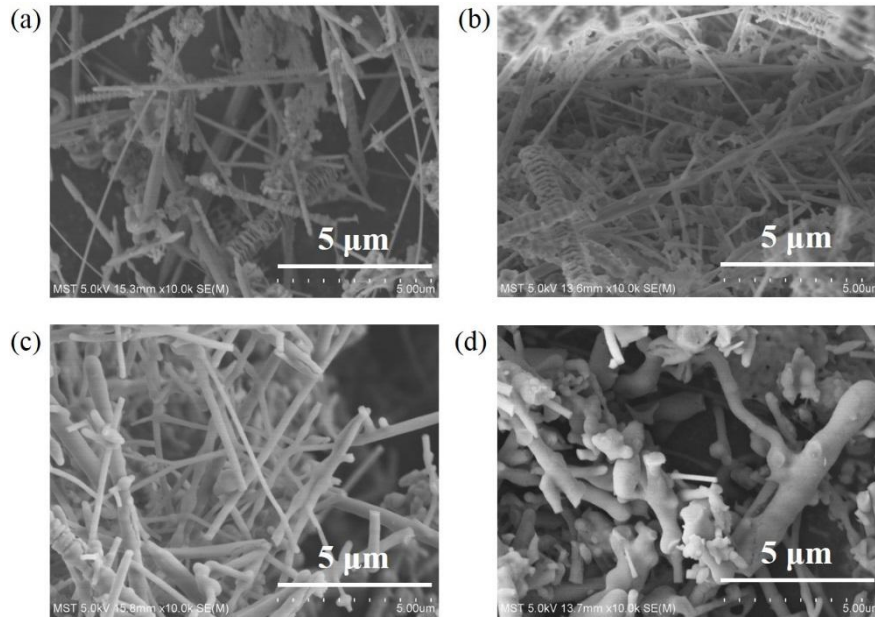
2
3
4
Fig.2 The pore size distribution of the support

1 **Fig.3**



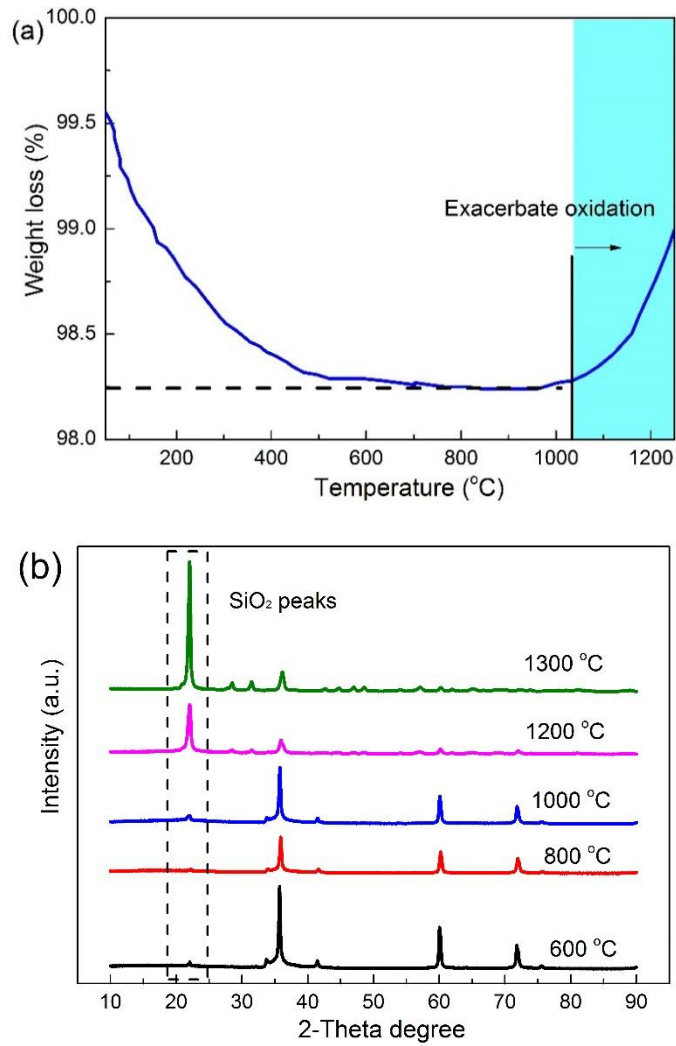
2
3
4 **Fig.3** (a) the relative resistance Vs the ϕ/d_p (b) three strategies for the sub-layer (strategy A, strategy B and
5 strategy C) (c) the relative resistance of ceramic membrane from three different strategies.
6

1 **Fig.4**



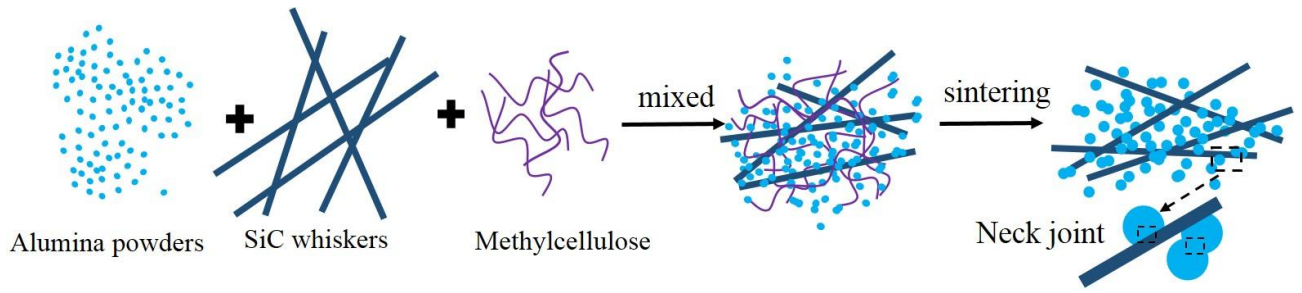
2 **Fig.4** The morphology of SiC whiskers sintered at different temperatures (a) 600 °C (b) 800 °C (c) 1000 °C
3
4 (d) 1200°C

1 **Fig.5**



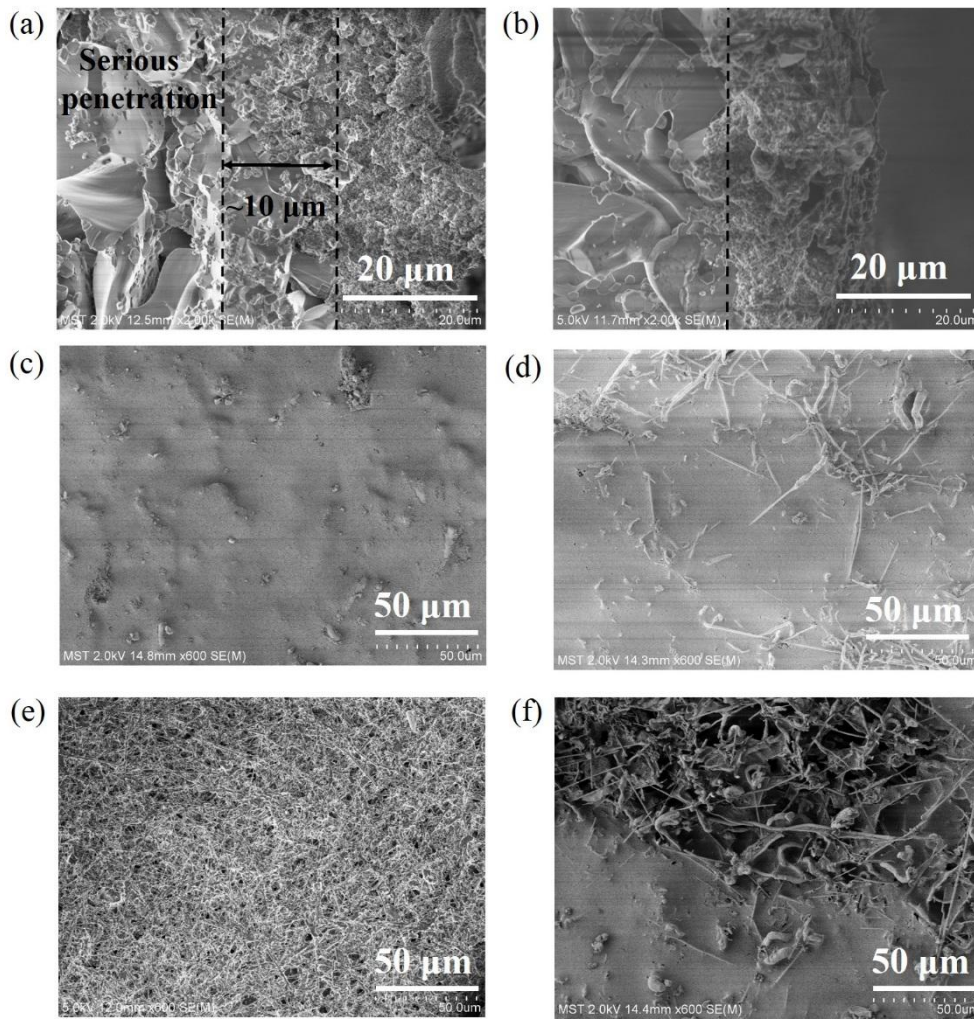
2
3
4 **Fig.5** (a) TG of the SiC whiskers (b) XRD patterns of the SiC whiskers at different sintering temperatures

1 **Fig.6**



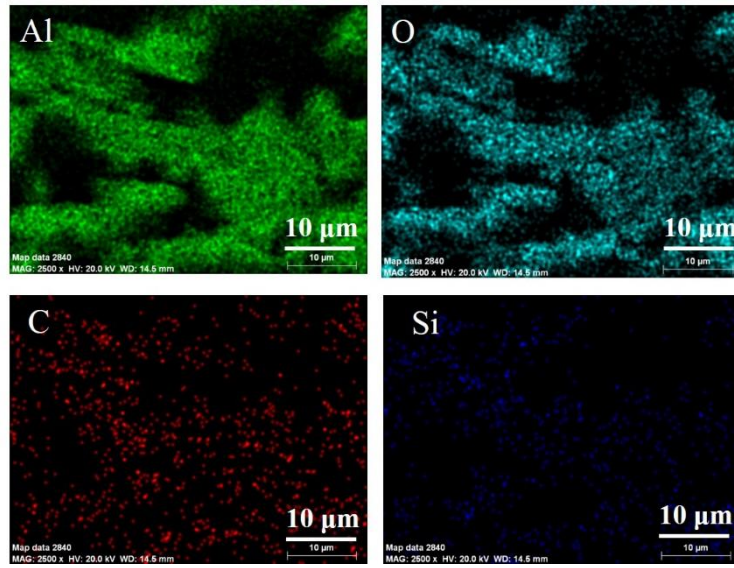
2
3 **Fig.6** Schematic illustration of the whiskers sintered with the aid of alumina powders with average particle
4 size of 300 nm
5

1 **Fig.7**



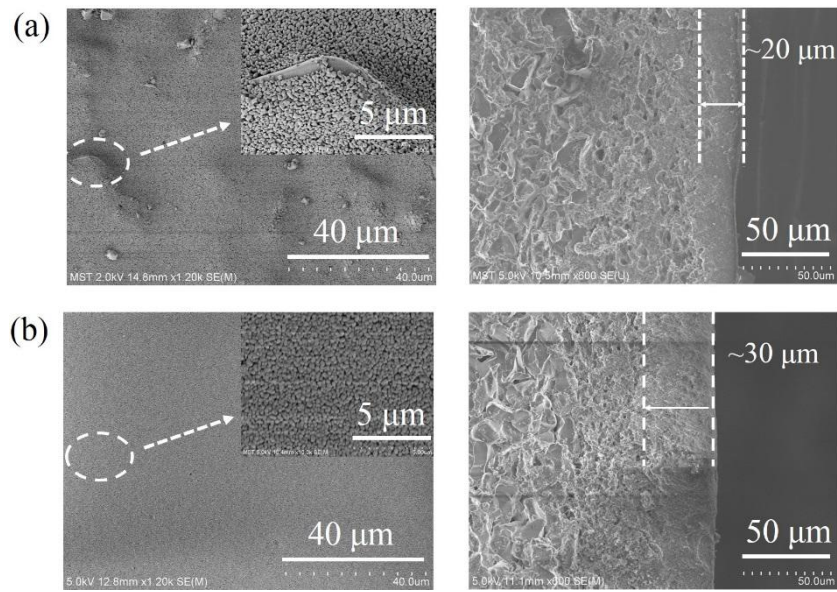
2
3 **Fig.7** The effect of SiC whiskers doping content on the ceramic membrane (a) Cross section of doping 0 wt.%
4 SiC whisker (b) Cross section of doping 10 wt.% SiC whiskers (c) 0 wt.% (d) 5 wt.% (e) 10 wt.% (f) 20
5 wt.%

1 **Fig.8**



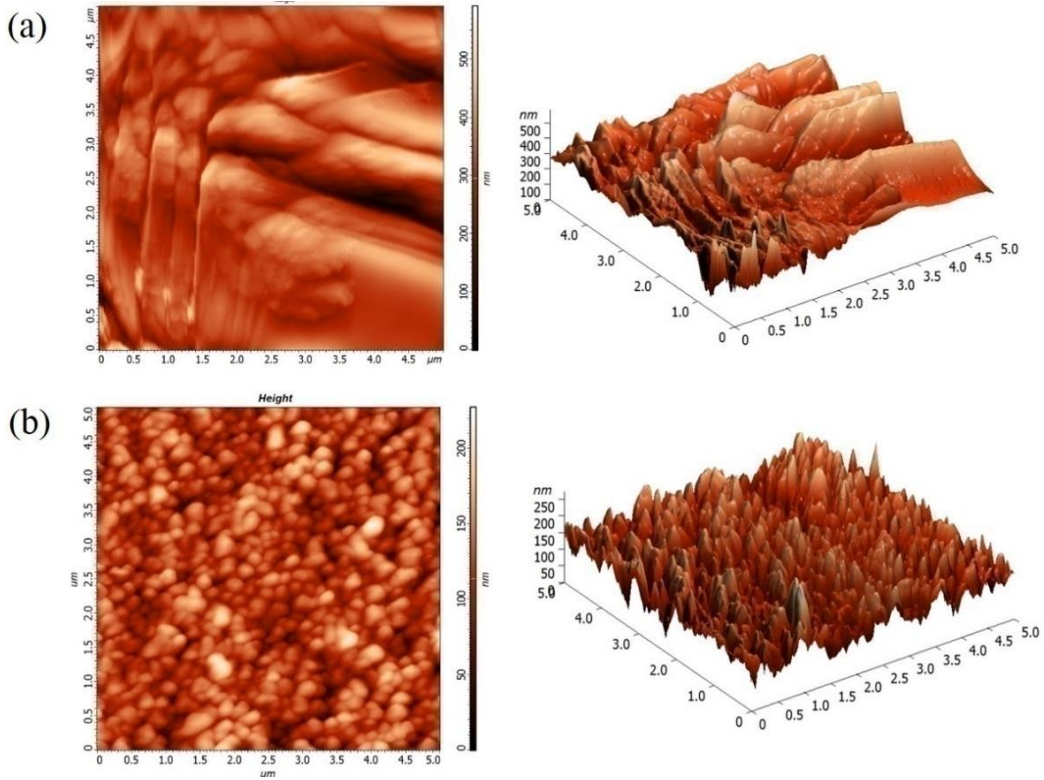
2
3 **Fig.8** The elements distribution on whisker membrane surface (Al, O, C and Si)

1 **Fig.9**



3 **Fig.9** The effect of the dipping time on structure of membrane surface and cross section (a) 60 s (b) 90 s

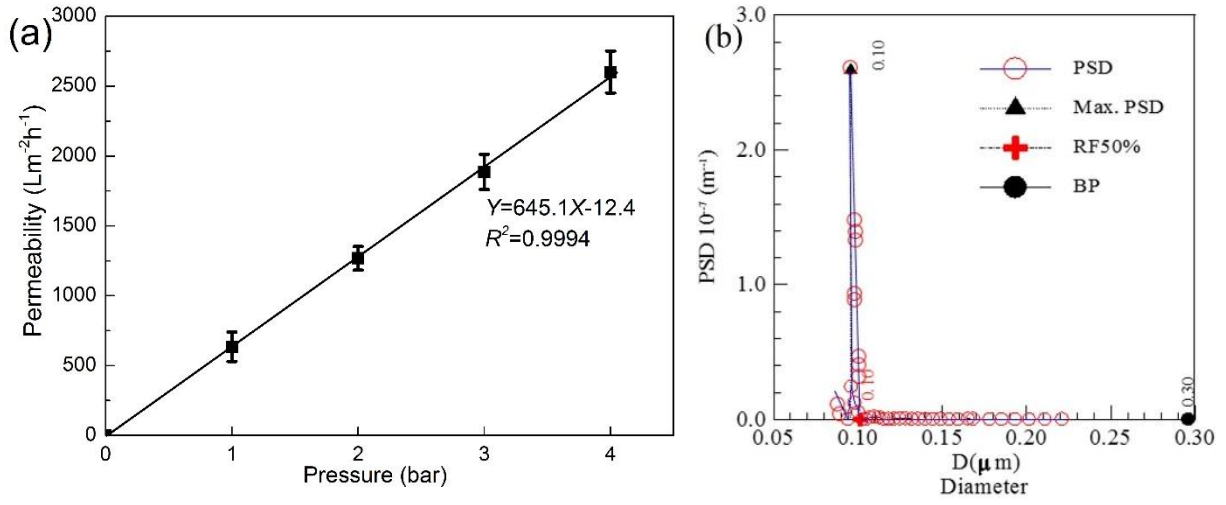
1 **Fig.10**



2
3 **Fig.10** The roughness membrane surface (a) Whisker layer (b) Alumina layer

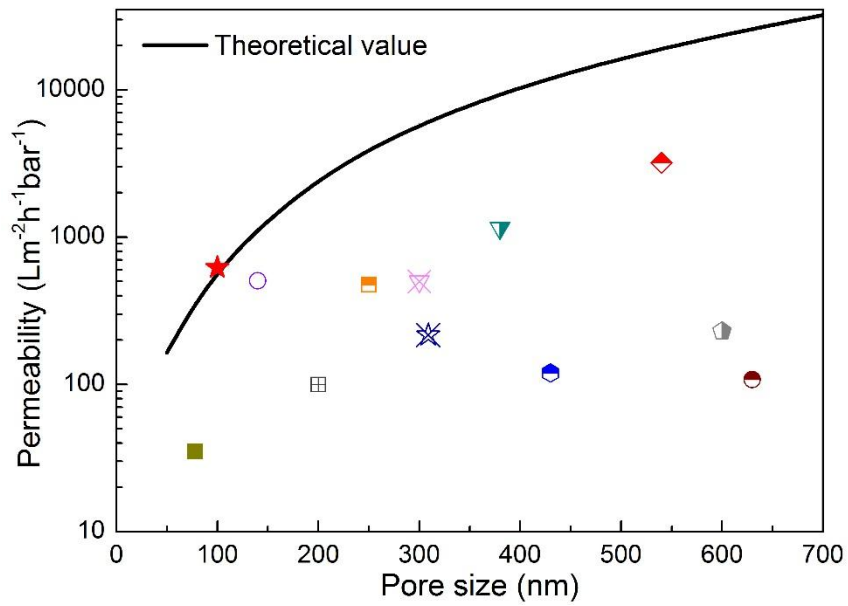
4

1 **Fig.11**



2
3 **Fig.11** The performance of the WHCM (a) Permeability (b) Pore size distribution

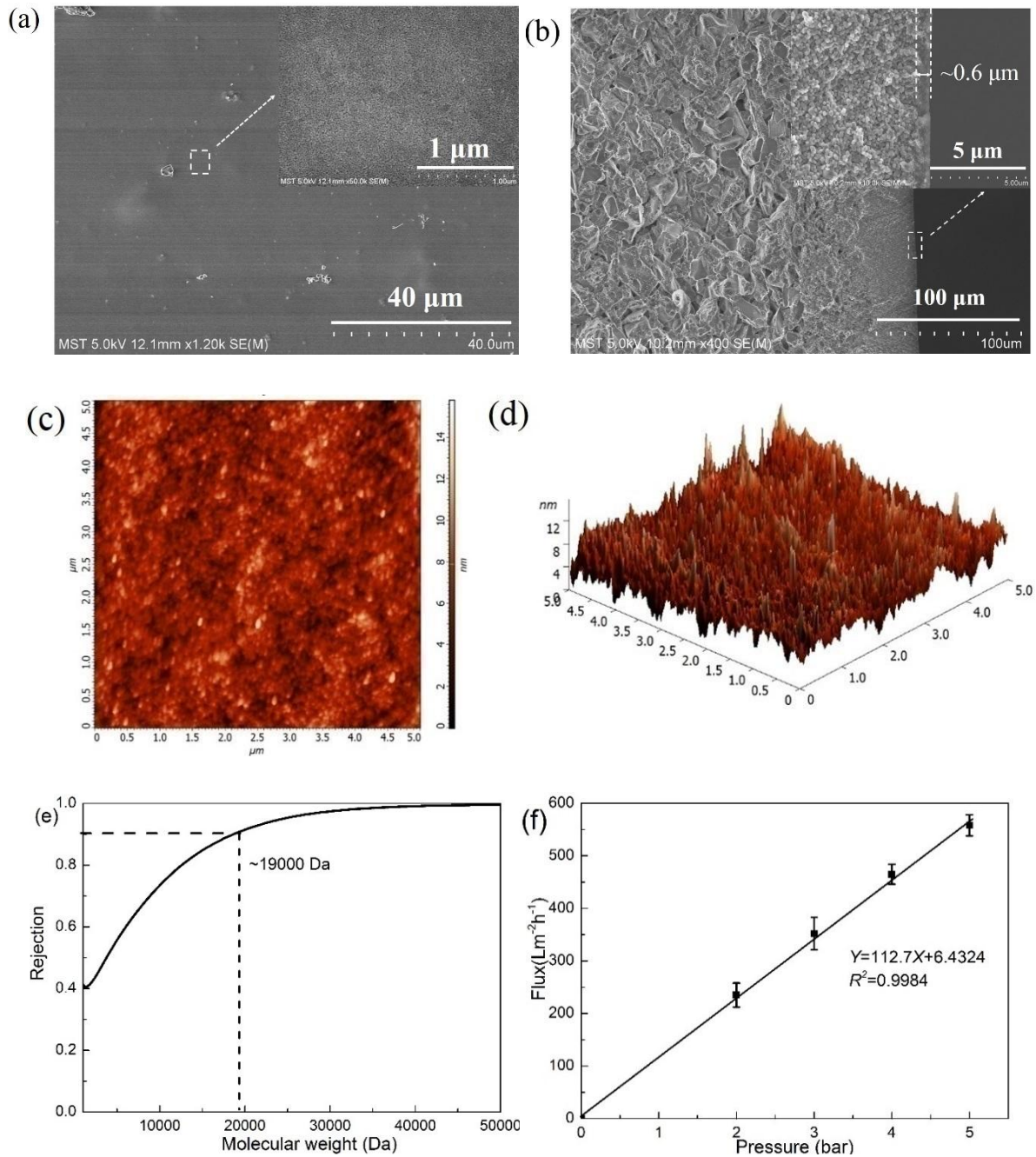
1 **Fig.12**



2 **Fig.12** The performance of the WHCM compared with the literatures

3
4
5
6
7
8
9
10
11
12
13
14
15
16
17
18
19
20
21
22
23
24
25
26
27
28
29
30
31
32
33
34
35
36
37
38
39
40
41
42
43
44
45
46
47
48
49
50
51
52
53
54
55
56
57
58
59
60
61
62
63
64
65

1 **Fig.13**



6 **Fig.13** The SEM images of the UF membranes (a) The surface images (b) The cross section (c) 2D-AFM
7 image (d) 3D-AFM image of membrane surface (e) Rejection performance (f) Permeability
8
9

1 **Fig.14**

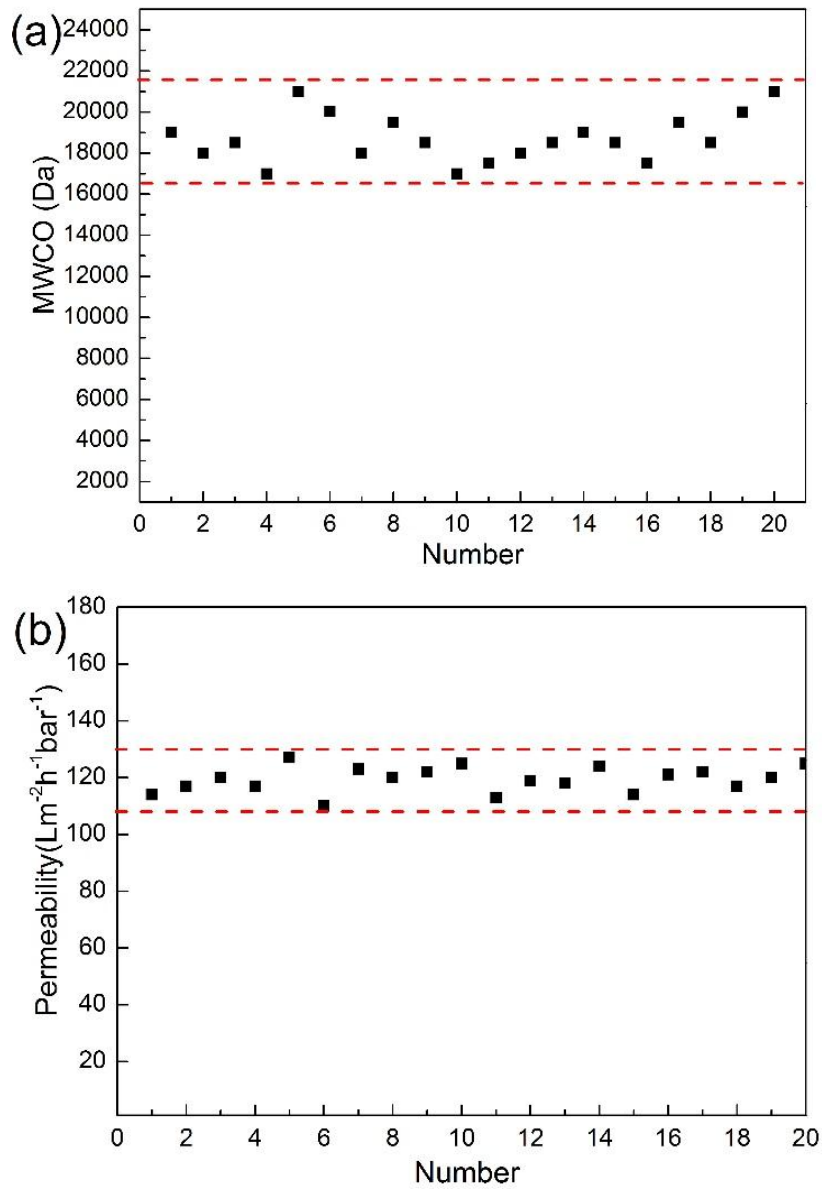


Fig.14 The repeatability of the UF membranes (a) MWCO (b) Permeability